



## Electrical resistivity and microstructural properties of concrete materials in conditions of current flow

D.A. Koleva<sup>a,\*</sup>, O. Copuroglu<sup>a</sup>, K. van Breugel<sup>a</sup>, G. Ye<sup>a</sup>, J.H.W. de Wit<sup>b</sup>

<sup>a</sup> Delft University of Technology, Faculty of Civil Engineering and Geosciences, Section Materials and Environment, 2628 CN Delft, The Netherlands

<sup>b</sup> Delft University of Technology, Faculty of Materials Science and Engineering, Section Surfaces and Interfaces, Mekelweg 2, 2628 CD Delft, The Netherlands

### ARTICLE INFO

#### Article history:

Received 13 July 2006

Received in revised form 18 April 2008

Accepted 22 April 2008

Available online 13 May 2008

#### Keywords:

Electrical properties

Ion transport

Pore structure

Pulse current

### ABSTRACT

The concrete matrix has a significant contribution to the global performance of reinforced concrete. In conditions of current flow (as in the case of impressed current cathodic protection (ICCP)) the concrete bulk material undergoes changes in chemical composition, electrical properties and microstructure, thus influencing the overall response of the reinforced concrete system. Aiming at optimization of the ICCP technique, a comparison study is carried out in this contribution between pulse and conventional ICCP in terms of bulk matrix (concrete) response to applied electrical current regimes. Ordinary Portland cement concrete blocks were cast, differing in experimental set-up and chloride concentrations. All specimens were subject to resistance monitoring and ion concentrations determination. The favourable effects of pulse cathodic protection current flow on the concrete matrix were additionally explained by microstructural analysis of the specimens. It is found out that physicochemical changes due to ion transport as well as electrical properties of the concrete matrix are attributed to the structural alterations of the pore space induced by the cathodic protection current.

© 2008 Elsevier Ltd. All rights reserved.

### 1. Introduction

Corrosion resistance of reinforced concrete structures is of significant importance in salt bearing environments such as in marine or coastal areas. Generally, the steel in hardened concrete is protected by a passive layer, maintained intact in the high alkalinity of the bulk matrix (normally pH = 12.5–13.5). The pH in concrete is established by the equilibrium between Ca(OH)<sub>2</sub>, calcium silicate hydrate (C–S–H) and the pore solution [1]. However, when sufficient aggressive ions (e.g. sulphate and chloride from sea water or chloride from de-icing salts) have penetrated to the reinforcement or when the pH of the pore solution drops to low values due to carbonation, the protective film is destroyed and the reinforcement steel de-passivated. This enables corrosion of the steel, volume expansion due to formation of corrosion products and subsequent cracking and spalling of concrete from the reinforcement.

Impressed current cathodic protection (ICCP) has been used for corrosion protection in reinforced concrete since the 1970s. So far it is proven to be the only technique that is able to minimize or stop corrosion in salt contaminated environments [2]. With ICCP, polarization of the steel reinforcement is achieved by supplying direct current (DC) to the steel embedded in concrete structures, making the occurrence of corrosion thermodynamically impossi-

ble. The repulsion of aggressive anions (e.g. chloride) which takes place along with the protection itself is beneficial as far as corrosion risk for the steel is concerned. An excessive overprotection current, however, will result in alkali ions (K<sup>+</sup>, Ca<sup>2+</sup>, Mg<sup>2+</sup>) accumulation at the steel/rebar interface, thus causing softening of the C–S–H gel, alkali silica reaction (ASR), bond degradation [3], micro-structural alterations and micro-cracking [4]. The main negative effect in terms of concrete microstructure is enlarging the gap between cement paste and aggregate in the interfacial transition zones (ITZs), thus yielding micro-cracks. Furthermore, concrete electrical resistance increases with aging. As previously investigated by the authors [5], microstructure alterations in cement-based materials yield non-uniform electrical properties and thereby possibly result in disturbance of the electrolytic path (i.e. the current demand is increasing). This constitutes an additional feature that should be overcome in engineering applications of the cathodic protection (CP) techniques.

This study explores the applicability of pulse current as an alternative to conventional steady DC current for corrosion protection. The investigation was performed on different stages: shorter testing periods are reported in [6], while the present work comprises results from the total duration of the test (210 days of cement hydration). The paper focuses on the influences of conventional and pulse CP current on ion transport, on electrical resistivity and on microstructural alterations in the concrete specimens. In particular, the study aims at correlating electrical properties with the concrete microstructure changes (in pore structure and the

\* Corresponding author. Tel.: +31 15 278 7451; fax: +31 15 278 8162.

E-mail address: [D.A.Koleva@TUDelft.nl](mailto:D.A.Koleva@TUDelft.nl) (D.A. Koleva).

ITZ) associated with the CP current. The research reveals that cost-effective pulse CP applications can successfully minimize the side effects on material structure and promote beneficial ion diffusion and migration, while more efficiently overcoming the concrete resistance and thus suggesting better performance compared to conventional CP current applications.

## 2. Experimental materials and methods

### 2.1. Materials

Concrete prisms ( $100 \times 100 \times 300$  mm) were cast using Ordinary Portland Cement CEM I 32.5, sand and gravel (ratio 1:2:4, aggregate size ranging from  $125 \mu\text{m}$  to  $16$  mm), and a water-to-cement ratio (w/c) of 0.6. The specimens were de-moulded 24 h after casting and conditioned in a fog room (98% RH and  $20^\circ\text{C}$ ) for a curing period of 60 days. Afterwards they were maintained in a climate room (50% RH,  $20^\circ\text{C}$ ) until the end of the testing period (210 days). Table 1 indicates the differences in compositions between the three groups of specimens. Group D used de-mineralized water as mixing water, whereas 1.25 M NaCl solution was used for the group N. Half of the DN specimen was mixed with de-mineralized water and the other half with 1.25 M NaCl solution.

The specimens were subjected to no-current, pulse CP and conventional CP current flow (regimes and specimen designation also indicated in Table 1). The design of the DN group aims at monitoring ion transport due to concentration gradient (in no-current condition) or ion migration due to the applied CP current (under pulse or steady CP current condition). Mixed metal oxide (MMO) titanium plates were placed (within the casting process) on both sides of the prisms for applying the electrical current; five MMO titanium pins were embedded equidistantly at 90 mm depth for monitoring the voltage drops along the longitudinal direction of the prisms.

Each concrete prism comprises several sections, designated as A and B, which account for a certain part of the prisms in terms of geometry (A3 on the side of the positive pole, B3 on the side of the negative pole, while A4 and B4 are the middle sections). For specimens DN, the designation of sections A (s. A) and B (s. B) also accounts for the concrete mixture i.e. s. A are initially free of chlorides, while s. B are cast with chlorides (s. B use same mixture as for specimens N). Designations A(ed+) and B(ed-) denote for the edge portions of the specimens (schematically illustrated in Table 1). Relevant to the microstructural analysis in Section 3.4, sections A (s. A) present averaged parameters for A3 and A(ed+), while sections B (s. B) present the averaged parameters for B3 and B(ed-). In terms of regimes of conditioning, no-current condition is denoted as 'rest', conventional and pulse CP current coded as 'DC' and 'pDC', respectively.

### 2.2. Electrical resistance measurements and CP current regimes

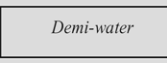
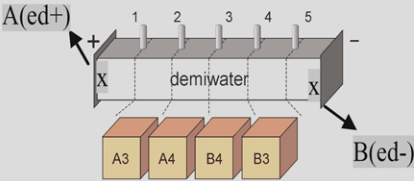
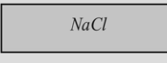
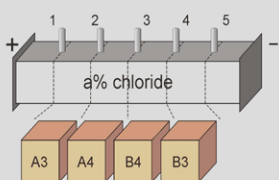
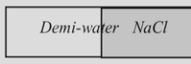
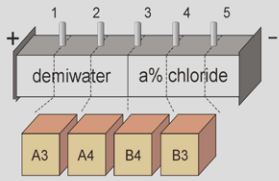
The resistance measurement was performed by AC 4 pin method in a certain regime (Tables 1 and 2). The advantage of the AC

**Table 2**

Technical specification: resistance monitoring and CP current regimes

Resistance measurement	Cathodic protection current
Measuring current 100 $\mu\text{A}$ balanced alternating square wave	DC current: 100 $\mu\text{A}$ (per cell)
Frequency: 120 Hz	Current source impedance: 300 kOhm
Current source impedance >10 MOhm	Pulse DC: 1 kHz
Voltage diff. input range: max $\pm 4$ V, 12 bit A/D conversion	Duty cycle 12.5–50%
Voltage diff. input impedance >100 MOhm	

**Table 1**  
Experimental set-up

Specimen code	Composition	Experimental set-up	Experimental conditions and specimens code		
			Rest	DC	pDC
<b>D</b> (x 9 specimens)	 (mixed with demineralised water)		<b>Drest</b> x3 specimens	<b>DDC</b> x3 specimens	<b>DpDC</b> x3 specimens
<b>N</b> (x 9 specimens)	 (1.25M NaCl solution as mixing water)		<b>Nrest</b> x3 specimens	<b>NDC</b> x3 specimens	<b>NpDC</b> x3 specimens
<b>DN</b> (x12 specimens)	 (NaCl concentration differs by sections)		<b>DNrest</b> x4 specimens	<b>DNDC</b> x4 specimens	<b>DNpDC</b> x4 specimens

methods in principle is that the mean value of the AC current is 0, i.e. the polarization effects due to the measurement could be minimized, thereby providing relatively high accuracy. The measurement was performed via the plates and pins embedded in the specimens (see Table 1). Thus several potential differences can be recorded, depending on the configuration. A multiplexer is used to select a specific section from a number of cells. Another multiplexer selects two electrodes (pins) to measure the potential difference. The resistance for each section of the prisms (sections A and B, Table 1) is then computed from the applied current and the recorded potential difference. The hereby used AC 4 pin (or 2 pin) method is a generally accepted technique for monitoring concrete electrical resistivity [7,8]; the method is also previously used by the authors and results are reported for mortar specimens [9].

The current supply (CP current of 10 mA/m<sup>2</sup>) was involved in two regimes, i.e. DC and pulse DC. The electrical current was applied to the side electrodes of the cells (the side MMO plates, Table 1), with one connected to the current source and the other to ground. Thus, a model regime of CP application was achieved. The main objective was to monitor the bulk concrete matrix response to electrical current flow (both steady and pulse DC) as in the event of ICCP. The specification for the resistance monitoring and the CP current regimes are given in Table 2.

### 2.3. Chemical analysis

Chemical analysis was performed for the *different sections* (sections A and B, Table 1) of the specimens at 14, 50, 128 and 210 days of cement hydration. Additionally, ion concentrations were determined at 64, 86 and 109 days of hydration for the specimens under the three technical regimes (rest, DC and pulse DC) by *drilling cores* (core diameter 15 mm), thus monitoring the changes in ion concentration for a specific section in one and the same specimen with time (the holes from the drilled cores were sealed with epoxy resin to prevent environmental influence to the remaining matrix of the specimen). The samples for chemical analysis (including determination of hydrated cement and hydrated water) were prepared according to ASTM C114-77 (wet chemical measurement of chloride concentrations using Volhard titration method). For the water-soluble chloride, the analysis conforms to ASTM C1218, for the acid-soluble chloride according to ASTM C1152. Alkali ions concentrations were determined by plasma spectrometry using Inductive Coupled Plasma spectrometer (ICP-AES). The chemical analysis aims at monitoring ion transport associated with diffusion and migration under electrical field (DC and pulse DC).

### 2.4. SEM imaging and pore structure analysis

Section images of the specimens were obtained by scanning electronic microscopy (SEM) in backscattered electrons mode (BSE) and at random locations on polished sections for each group of the concrete specimens. The physical size of the reference region of each image is 226  $\mu$ m in length and 154  $\mu$ m in width, with the resolution of 0.317  $\mu$ m/pixel (corresponding to a magnification of 500 $\times$ ). The original BSE image is segmented by applying a grey-level threshold to create a binary image reflecting the pore phase. The binary image is then subjected to quantitative image analysis for derivation of structural parameters.

Further, the combination of SEM imaging and quantitative image analysis allows deriving structural information of the pore space, such as porosity and critical pore size. On the basis of mathematical morphology transformations, pore size distribution can be obtained by using a sequence of similarly shaped structuring elements of increasing size [10]. In this study, the so-called 'opening distribution' is used whereby the binary image is opened by a

series of squares of increasing size. The opening distribution curve of pore space is obtained by plotting the pore area fraction after an opening operation versus the linear dimension of the structuring element. This gives a type of size classification in the case of an interconnected structure such as the pore space in concrete. For more details on the image analysis, relevant also to this work, please see [7,8,11].

## 3. Results and discussion

### 3.1. Electrical properties: changes due to cement hydration and CP current

The electrical resistivity of concrete is claimed to be one of the main parameters characterizing the possibility of displacement of charged particles under the influence of an external electrical field or under the influence of concentration gradients. The moisture content in concrete is the major factor that determines electrical resistivity. The concrete resistivity however (reciprocal of conductivity) is also characterized through the motion of ions such as Na<sup>+</sup>, K<sup>+</sup>, OH<sup>-</sup>, SO<sub>4</sub><sup>2-</sup>, Ca<sup>2+</sup> in the pore solution. In concrete, ionic (or electrolytic) conduction is the main phenomenon of electricity transport [12]. Thus, the value of concrete resistivity (conductivity respectively) could be also influenced by the ions concentration in the pore system. For example, the electrical conductivity can be correlated with the concentration of aggressive ions, such as Cl<sup>-</sup>, being a main cause for pitting corrosion in reinforced concrete. Some studies claim that the chloride ions will reduce the resistivity of wet concrete (i.e. increase concrete conductivity) and thus lead to corrosion risk [13,14]. Others report that reinforcement corrosion can be predicted from concrete resistivity, taking into account that chloride diffusivity is proportional to concrete conductivity [15]. An inversed correlation between concrete resistivity and chloride diffusion rate is found in [13,16]. Moreover, according to [13] the corrosion rate is inversely proportional to the concrete resistivity. These relationships, however, are not always straightforward, i.e. high concrete resistivity does not always mean low corrosion risk. A major contributing factor to the development of concrete electrical resistivity is the altered pore structure in the presence of chlorides (which also holds for conditions of electrical current flow), which will be discussed in the following sections.

#### 3.1.1. Monitoring electrical resistivity

Concrete electrical resistivity generally increases with time, as a result of cement hydration, a mechanism involved in all hereby investigated specimens. For the D, N and DN specimens, subjected to pulse and conventional CP current (designation in Table 1), the electrical properties are additionally influenced by the electrical current flow through the specimens. For specimens N and DN in rest as well as in all current regimes, there will be a combined influence of electrical current and/or chlorides in addition to the general cement hydration.

Resistance monitoring was performed during a period of 210 days of cement hydration. The total electrical resistivity and local resistivity at various sections of the specimens (Table 1) are calculated using the equation:  $\rho = RA/l$ , where  $\rho$  is the resistivity (Ohm-cm),  $R$  is the resistance (Ohm),  $A$  is the cross section area (cm<sup>2</sup>) and  $l$  is the length (cm). Fig. 1 depicts the evolution of total electrical resistivity for all groups in different technical conditions, i.e. in rest conditions (only cement hydration is involved), under pulse and conventional CP current with the current flowing through the cell as an additional influencing factor. Fig. 2 presents the changes in electrical resistivity for various sections in all groups of specimens under these technical conditions.

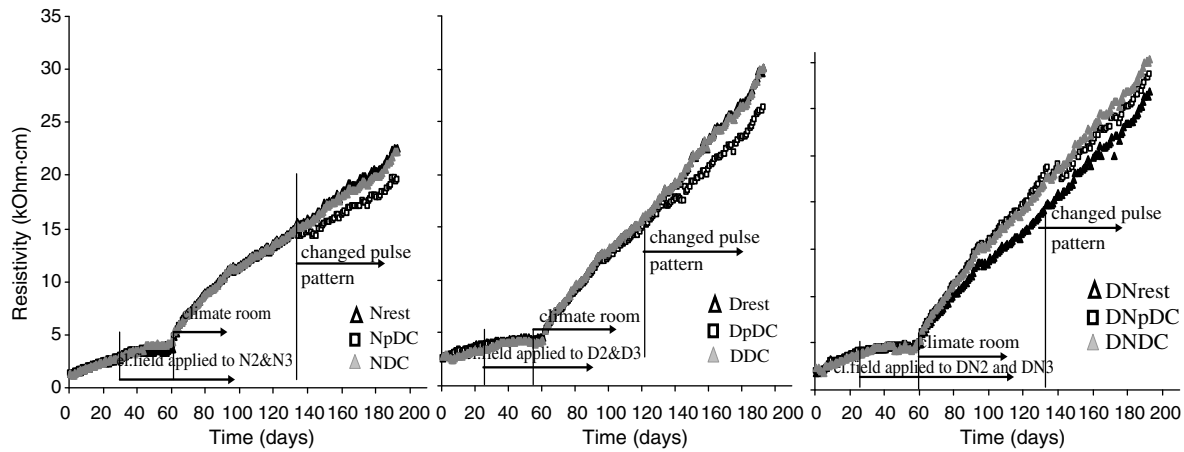


**Fig. 1.** Evolution of total resistivity vs. time (days of cement hydration) for different concrete specimens (D- mixed with demineralized water, N- mixed with 1.25 M NaCl solution, DN- half-to-half combination of D and N) under three technical conditions: rest- no-current conditions, pDC- under pulse CP current, DC- under conventional CP current. Details of the experimental set-up are indicated in Table 1.

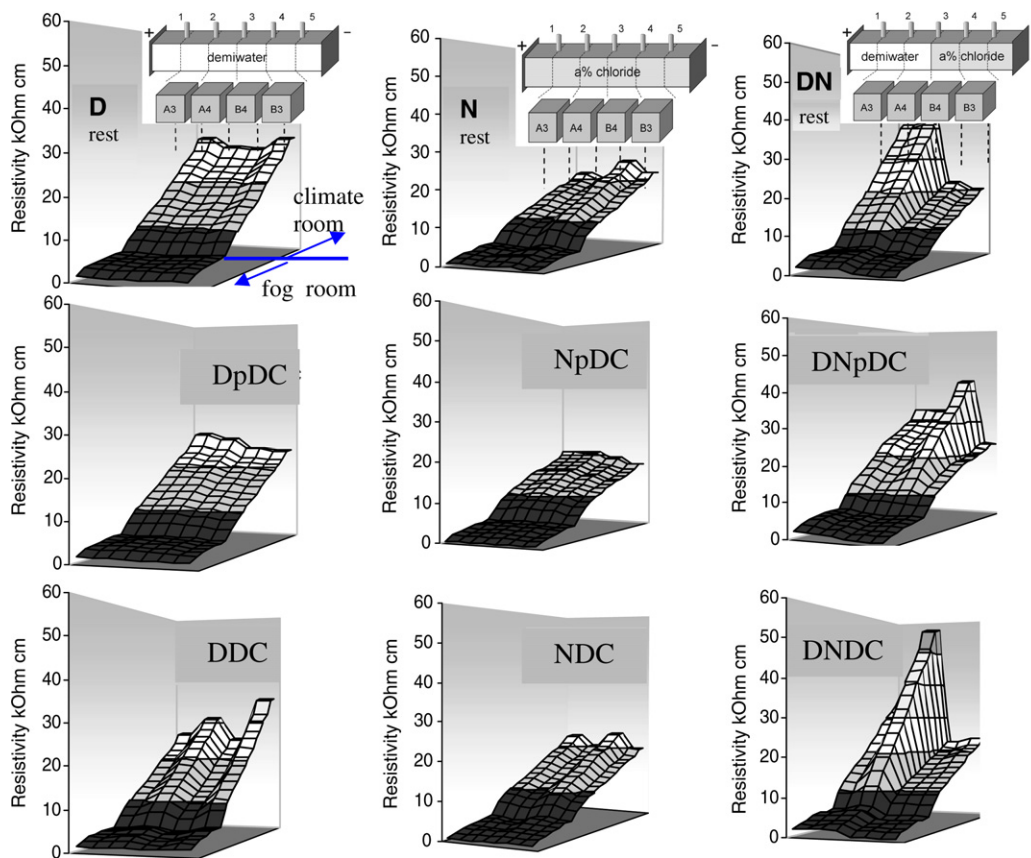
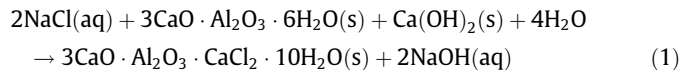


**Fig. 2.** Evolution of electrical resistivity with time of cement hydration for various sections (see Table 1) in concrete specimens under no-current (denoted as rest specimens), conventional CP (DC specimens) and pulse CP (pDC specimens) techniques.

### 3.1.2. Electrical resistivity in rest (no current) conditions

In the initial testing period of 30 days of cement hydration, all specimens were in the same condition (fog room) without CP application; during this period, only the chloride ions (for specimens N and DN) play a role in addition to cement hydration. Fig. 1 reveals that during this initial period all specimens follow the same pattern of resistivity increase, despite the significant NaCl concentration (1.25 M NaCl solution used as mixing water) in groups N and DN. The fact is attributed to the accelerated cement hydration in case of NaCl additions, represented by the following chemical reaction:



As a consequence, Friedel's salt is formed ( $3\text{CaO} \cdot \text{Al}_2\text{O}_3 \cdot \text{CaCl}_2 \cdot 10\text{H}_2\text{O}$ ), accompanied by release of NaOH, leading to a pH increase in the pore solution. This will further accelerate the hydration process and consequently modify the pore structure towards a finer pore size distribution, as will be further demonstrated by the pore structure analysis (Section 3.4). The chloride ions promote cement hydration and reduce the pore connectivity, hence, the electrical resistivity for all of the specimens during the first 30 days of testing



are similar and do not show a significant dependence on ion concentrations.

### 3.1.3. Electrical resistivity in conditions of electrical current flow

The electrical current (simulating CP current) was applied to certain groups concrete specimens (designation in Table 1) after 30 days of cement hydration and aimed at investigating the relationships between electrical properties and microstructure changes induced by the current flow. Figs. 1 and 2 reveal that in fog room conditions, all specimens show a smooth and gradual pattern of climb of the electrical resistivity. However, the electrical current is influencing the cement hydration as the amount of hydrated cement in some sections of specimens DN (half-to-half mixed specimens) is slightly higher than those in no-current conditions. This is attributed to enhanced ion migration which takes place along with the ion transport due to concentration gradient in the DN specimens. From this point of view, the pulse CP achieves better performance than the steady current, which will be further discussed in Section 3.2.

Since 60 days of cement hydration, all specimens were placed in climate room (50% RH). As expected, the electrical resistivity shows a considerable shift towards higher values (the specimens were drying out). The influences of current flow on electrical properties for specimens D and N are lower compared to specimens DN, the latter showing a significant increase in electrical resistivity due to the applied current (Fig. 1). The reason is that the  $\text{Cl}^-$  concentration gradient in the DN specimen additionally promotes ion transport and accelerates the hydration process. Changing the pulse pattern (see Table 2 and Fig. 1) at about 120 days leads to a slight decline in the resistivity for pulse current conditions (the latter trend of decline becoming more obvious at later stage). At the end of the testing period (210 days in Fig. 1), specimens DN revealed the highest electrical resistivity, whereas specimens N, the lowest. The difference of about 5–15 kOhm cm between specimens D (free of chlorides) and N (with chlorides) is not dramatic taking into account the considerable chloride concentration in specimens N (2.6% total and 1.87% free chloride per dry cement weight). The literature recommends chloride threshold values of 0.2–2.0% by mass of binder [17]; ACI 201.2R-77 suggests a limit of 0.10–0.15% free chloride by weight of cement for above ground structures. Hence, the chloride concentration in the investigated concrete (groups N and DN) is relatively high. However, the recorded electrical resistivity for these specimens (>20 kOhm cm) is also acceptable in view of the recommended thresholds for evaluating corrosion risk (Table 3). It is evident that caution should be bestowed on interpretation of such experimental results. In other words, the high electrical resistivity of specimens N and DN would not account for low corrosion risk, since the high chloride concentration will certainly cause localized corrosion if reinforcement was present in these latter specimens. Hence, a direct correlation between electrical resistivity and chloride concentration cannot be derived.

### 3.1.4. The combined effect of electrical current flow and concentration gradient on concrete electrical resistivity

Fig. 2 depicts the influence of electrical current flow and concentration gradient (specimens DN) on the concrete electrical resistivity for the total duration of the test (210 days). As seen from the plots (also Fig. 1) the concrete electrical resistivity is not signifi-

cantly influenced by concentration gradients for the period of fog room curing (up to 60 days of cement hydration). This implies that the high RH of the surrounding environment plays a decisive role. After this stage (in climate room, but still with high humidity of 50% RH) the influence of ion diffusion and migration becomes more evident, particularly confirmed by the changes of electrical resistivity at different sections of the prisms (Fig. 2). A comparison study between the specimens without (rest) and with electrical current application (DC and pDC specimens) allows separately evaluating the influences of ion migration and electrical current. For specimens without current application (the rest groups), the only influencing factor is cement hydration (i.e. aging) and for specimens DN, also including concentration gradient. Fig. 2 clearly reveals the non-uniform values of resistivity for all the specimens under steady current, particularly in DDC, NDC and DNDC specimens. This can be attributed to non-uniform binding/de-binding mechanism of chlorides in the cement matrix (as already reported in [5,9]) and to the alterations in pore connectivity in the bulk material.

When there is no concentration gradient (i.e. D and N specimens), steady DC (conventional CP) current increases the electrical resistivity, compared to the rest conditions. Pulse DC current (specimens DpDC and NpDC) exerts slight influences on the electrical properties; lower resistivity is recorded for both groups in the sections B (around the negative pole of the cells). Basically, decline in electrical resistivity could be explained by two main reasons, i.e. the presence of micro-cracking or easy water and ion transport. In the former case, damaged microstructure will further reduce overall resistance of the concrete material and consequently increase the conductive paths. The latter case is strongly related to structural parameters of the bulk concrete matrix. Microstructure analysis (Section 3.4) demonstrates higher extent of detrimental effects by the steady DC current compared to the pulse current. The favourable structural alterations, together with possible electro-osmotic effects [20] are underlying the positive effects of the pulse current regime.

The mechanisms are more complicated for the mixed specimens (DN) under steady and pulse DC (specimens DNpDC and DNDC). Here, the steady current significantly increases the resistivity in the middle sections A/B, in contrast to the less dramatic effects of the pulse DC (Fig. 2), exhibiting behaviour, similar to rest conditions. It should be noted that the section B3 (close to the negative pole of the cell, with NaCl addition, Table 1, Fig. 2) in the pulse DC condition (specimen DNpDC) shows higher electrical resistivity than sections A (initially free of chloride). The phenomenon can be denoted to a considerably accelerated hydration process in section B (right half of the specimen) as result of enhanced ion migration under the influence of current flow. Chemical analysis (Section 3.3) of amounts of hydrated water by sections of the specimens provides supporting evidences. The favourable effect of pulse DC (compared to steady DC) is additionally envisaged by the much more uniform values of electrical resistivity among various sections of the specimen (see Fig. 2).

### 3.2. Hydration mechanism and electrical properties

Concrete has many special characteristics, including high alkalinity of the pore solution, high electrical resistivity and structure itself acting as a barrier for mass transport. All these features affect

**Table 3**  
Electrical resistivity thresholds for evaluation of corrosion risk in reinforced concrete structures

Empirical interpretation (after [18])		Interpretation using Gecor 6 device (after [19])	
>20 kOhm cm	Low corrosion risk	>100 kOhm cm	No risk
10–20 kOhm cm	Low to moderate corrosion risk	50–100 kOhm cm	Low corrosion risk
5–10 kOhm cm	High corrosion risk	10–50 kOhm cm	Moderate to high corrosion risk
<5 kOhm cm	Very high corrosion risk	<10 kOhm cm	Resistivity is not the controlling parameter

the electrical properties and hence influence the ion transport and current flow in concrete materials.

As well known, the hydration process in concrete results in the formation of calcium silicate hydrate (C–S–H), calcium hydroxide (CH), ettringite and other compounds. During hydration, the capillary pores are gradually filled up with hydration products and the solid phases form a rigid microstructure with increasing strength. Relevant to the present study, the presence of NaCl is involved in the hydration mechanisms, and thereby also influences the ion migration and electrical current flow through the specimens. Water plays a decisive role with respect to these transport processes and can be classified into different forms in the porous structure [21]: chemically combined (bound) water; interlayer water; absorbed (capillary) water. The amount of bound water can determine the degree and rate of cement hydration, hence is related to electrical resistivity and ease of ion transport.

### 3.2.1. Chemically combined water in conditions of current flow

The percentage of bound (hydrated) water for D specimen in rest conditions (Drest) is 18%, climbing to an average value of 25% at 210 days for the specimens under current flow (DDC and DpDC) (Fig. 3a). The plot depicts the amount of bound water at different sections (middle part and around the positively and negatively charged poles) for specimens D under steady (DDC) and pulse (DpDC) current, respectively. The percent of bound water is the highest in section B3 of specimens DDC and lowest in section B3 of specimen DpDC. These results correspond well to the electrical

resistivity measurements (Fig. 2). Hence, the amount of interlayer and capillary water in those sections is higher which determines the lower resistance. The same observations hold for samples N (with addition of NaCl) for both current regimes: the lower amount of bound water at the negative pole for specimens under pulse DC (NpDC, see Fig. 3b) corresponds to the lowest electrical resistivity for the same section. The higher bound water content in the middle section and in section B4 for specimen N under steady current (NDC) corresponds to higher electrical resistivity for the same section (Fig. 2).

The relationship between bound water content and concrete resistivity for the mixed specimen DN under pulse current regime (DNpDC) follows a similar trend as for specimens D and N, but additionally affected by ion transport as a combined influence of concentration gradient and electrical fields – Fig. 4.

### 3.2.2. The combined influence of NaCl and electrical current flow on cement hydration in terms of bound water

Sodium chloride increases the rate of hydration (higher electrical resistivity, respectively) for sections B (on the side of the negative poles) of all specimens, consequently higher percentages of hydrated water are recorded for these sections. The electrical current flow is additionally promoting cement hydration, especially under DC conditions, as evidenced by the chemical analysis for hydrated water (Fig. 4), revealing highest percentages of bound water in specimen DNDC. The specimens DN under pulse DC conditions (DNpDC) behave similarly to rest conditions (DN rest), with

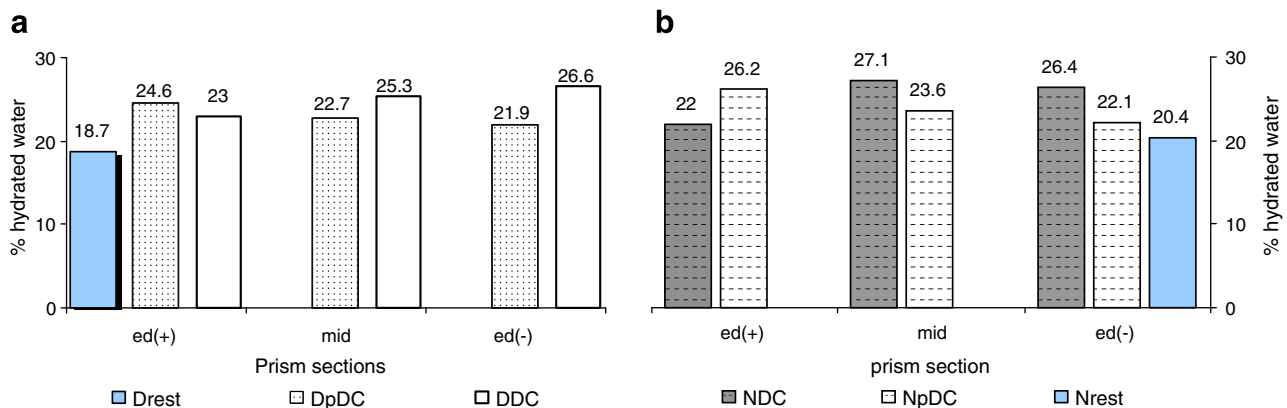


**Fig. 3.** (a) Distribution of bound (hydrated) water by sections (middle sections and charged poles) in% per dry cement weight in specimens D in rest conditions (Drest), under steady (DDC) and pulse (DpDC) current; (b) distribution of bound water (% per dry cement weight) in middle sections and charged poles, for samples N in rest conditions (Nrest), under steady (NDC) and pulse (NpDC) current.

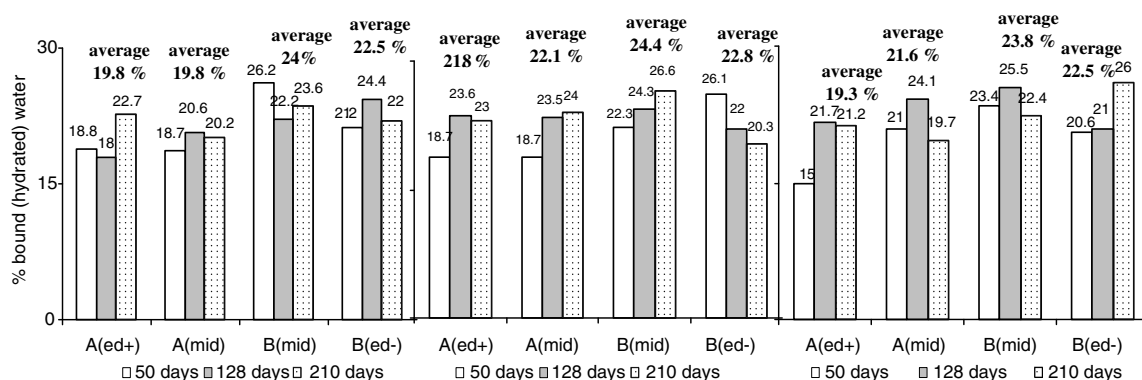


**Fig. 4.** Distribution of bound (hydrated) water by sections (middle sections corresponding to A4 and B4, hereby designated only as A(mid) and B(mid) and charged poles (designated A(ed+) and B(ed-), see Table 1) in% per dry cement weight in specimens DN in rest conditions (Drest), under steady (DNDC) and pulse (DNpDC) current.

slightly higher values of hydrated water in the middle section A and even lower values for the positively charged pole (A<sup>ed+</sup>). These phenomena will be further elaborated with respect to chloride-induced accelerated hydration and microstructural properties in what follows.

Specimens DN under steady current (DNDC) and no-current conditions (DNrest) exhibit similar behaviour in terms of larger variations in electrical resistivity by sections (Fig. 2). The amount of hydrated water is basically relevant to the amount of hydrated cement, and the sections with highest percent of hydrated water would correspond to the sections with highest resistivity, as recorded for specimens DNDC and DNpDC (Figs. 2 and 4). For specimen DN in rest condition, sections B3 and B4 contain higher amount of hydrated water (due to the chloride-induced acceleration of the hydration process), but exhibit lower electrical resistivity compared to sections A. In the advanced stage of hydration process, diffusion is the limitation reaction. When current flow is involved, the hydration process is accelerated (as in DNDC and DNpDC). The current flow influences the direction of ion transport: anions (chloride and OH<sup>-</sup> ions) should move to the positive pole, cations (Na<sup>+</sup>, K<sup>+</sup>, Mg<sup>2+</sup>) to the negative one. Chemical analysis, by sections of all specimens for all technical conditions, reveals higher mobility of chlorides under current flow, more pronounced for pulse conditions (DNpDC) – Fig. 5 (left) and no significant change in sodium concentrations by sections of the prisms – Fig. 5 (right).

### 3.2.3. Microstructural phenomena, related to the combined effects of cement hydration, current flow and ion transport mechanisms

The free ion movement in the concrete bulk matrix can generally undergo in counteracting streams, e.g. Na<sup>+</sup> ions are normally surrounded by water dipoles (hydration shell), and thus in conditions of current flow (as in specimen groups DC and pDC) they can migrate to the negative pole (set up in Table 1). In case of counter transport of OH<sup>-</sup> and Na<sup>+</sup> in the pore solution, water content will possibly be reduced at the negative terminal. Thus, the material microstructure is externally changed by the electrical current, due to the impact of the latter on ion and water transport. Moreover, the electrical properties of the different interfacial zones in the concrete matrix can be directly correlated with resistivity of the materials. According to [22], there are basically three types of paths in concrete structure, i.e. continuous conductive paths (CCPs), discontinuous conductive paths (DCPs), and 'insulator' conductive paths (ICPs), respectively. The CCPs consist of connected micro-pores, which could be a series of capillary cavities connected through pore necks. If the micro-pores are blocked by the cement

paste layers, these discontinuous pores constitute the DCPs. Apart from the DCPs and CCPs, the continuous concrete matrix composed of cement paste, acts as 'insulator' paths (ICPs) in the concrete system. All these paths contribute to the overall ion transport and thereby to the electrolytic and current transport in the system. An enhanced ion movement will lead to faster hydration and filling up of the pore network. This explains the higher resistivity in section B4 of DN specimen under pulse current.

The involvement of electrical current (both steady and pulse) will stimulate the hydration process by accelerating ion transport, in this case, the conductive CCPs and non-conductive ICPs will transform from one to the other. In general, the portion of CCPs will decrease and DCPs increase with cement hydration and physico-chemical reactions. Hence, both current regimes will reduce the portion of CCPs and thereby increase the total electrical resistivity. However, in case of pulse current, with alternating periods of 'on' and 'off' current flow, there is a favourable mechanism of charge-discharge cycling, and the ions are prevented from 'piling up'. Hence the portion of conductive CCPs is more than that of the DCPs. This is supported by the much more uniform resistivity values at various sections in specimens under pulse DC compared to those under steady DC (Fig. 2) and ease of ion transport (mainly chlorides) – Fig. 5, which will be discussed in the following section.

### 3.3. Chemical phenomena: influence of cement hydration and electrical current regimes on ion transport

#### 3.3.1. Chloride binding mechanisms

When chloride ions penetrate through the concrete surface and ingress into the bulk material, part of them undergo chemical binding, part of them remain physically bound, and the others stay free in the pore solution. Bound chlorides can be released when carbonation takes place [23], therefore, bound chlorides can present corrosion risk as well. The chemical binding of chloride ions is a process of incorporation into the lattice of crystalline hydration products in the form of 3CaO · Al<sub>2</sub>O<sub>3</sub> · 3CaCl<sub>2</sub> · 10H<sub>2</sub>O and 3CaO · Al<sub>2</sub>O<sub>3</sub> · 3CaCl<sub>2</sub> · 32H<sub>2</sub>O. The amount of the tri-calcium aluminate phase (C<sub>3</sub>A) in the cement matrix has significant influence on the chloride binding mechanism and thereby on the amount of chlorides remaining free in the pore solution. Further, part of the free chloride ions bind by releasing equivalent amount of hydroxyl ions into the pore solution, the rest of free chloride ions bind without releasing OH<sup>-</sup> into the pore solution [24]. Thus, the formation of CaCl<sub>2</sub> for example causes dissolution of portlandite and generates hydroxyl ions in the pore solution. The rise of OH<sup>-</sup> ion concentration can

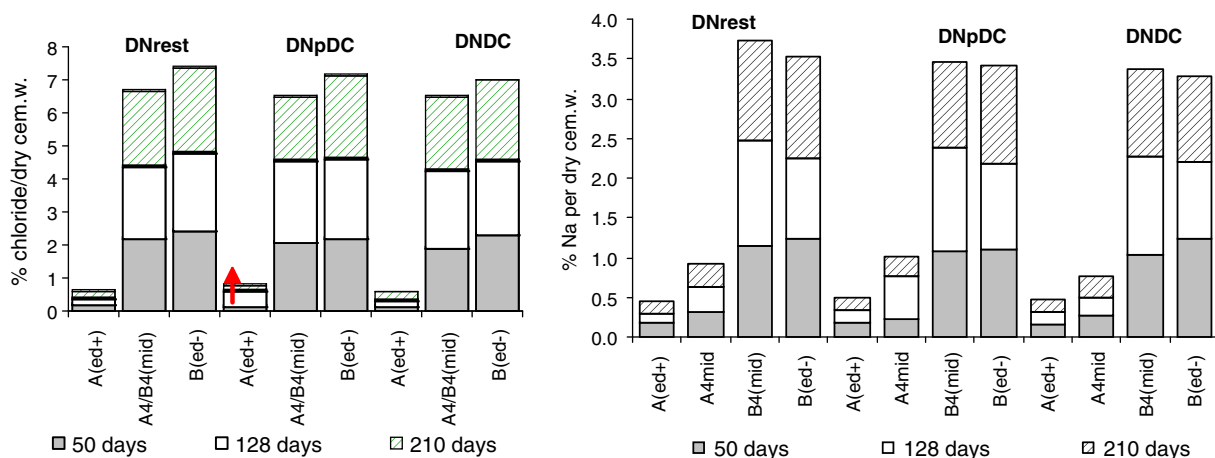


Fig. 5. Total chloride (left) and sodium concentration (right) in% per dry cement weight for the different sections of specimens DN in rest (DNrest), steady DC (DNDC) and pulse DC (DNpDC) conditions (sections designation in Table 1).

be alternatively explained by displacement of  $\text{OH}^-$  in the interlayers of the ferrite phases ( $\text{AF}_m$  hydrates) by the chloride ions from the pore solution. The unreacted  $\text{C}_3\text{A}$ , remained after preferential reaction with sulphates, reacts in the presence of excess of  $\text{Ca}(\text{OH})_2$  and forms  $4\text{CaO} \cdot \text{Al}_2\text{O}_3 \cdot 13\text{H}_2\text{O}$  ( $\text{C}_4\text{AH}_{13}$ ), and the meta-stable  $\text{C}_4\text{AH}_{13}$  can transform to other  $\text{AF}_m$  hydrates. The amount of  $\text{OH}^-$  ions that will exchange with the  $\text{Cl}^-$  ions depends on the number of sites available for ion exchange, or indirectly on the quantity of  $\text{AF}_m$  hydrates present in the hydrated cement [25]. It follows that the maximum limit of ion exchange will depend on the ion-exchange capacity of  $\text{AF}_m$  hydrates.

### 3.3.2. Ion exchange mechanisms in conditions of current flow

The aforementioned ion exchange mechanisms are slow in no-current conditions due to slow diffusion and ion transport. When electrical field is applied (as in the CP model regimes in this study), ion migration will take place along with diffusion mechanisms and consequently speed up all related chemical transformations. Hence, ion exchange is closely related to electrical resistivity properties of the specimens.

In addition to the chemical analysis (ion concentrations, hydrated water) of the concrete prisms by sections (Table 1, Figs. 4 and 5), monitoring was performed on cell couples (DC and pDC), in one and the same sections of the specimens by drilling cores, thus recording information for one and the same section of the prisms with time. Fig. 6 presents the chloride and alkali concentrations measured from drilled cores of the specimens DN at different stages of hydration. In the specimens under pulse CP current regime (DNpDC), the current flow is accelerating the ion transport towards sections A (initially free of chloride) where the ion-exchange capacity is higher, thus increasing the hydration rate and filling up of the pore system. It is followed by reduction in the portion of CCPs in the system and increased electrical resistivity. In

this case, the physicochemical process is taking place more uniformly throughout the specimens than the specimens under steady DC, evidenced by the local resistivity measurements (Fig. 2). This effect can be additionally proved by the lower and almost uniform chloride concentrations in specimen DNpDC at the middle part and negatively charged pole of the specimens, accompanied by a higher chloride concentration around the positively charged pole, compared to the specimens under steady DC current (Fig. 6a). Furthermore, when chloride ions diffuse through hardened cement paste,  $\text{Ca}(\text{OH})_2$  crystals are identified on the surface of the hydrated cement. This is due to the counter diffusion of  $\text{Cl}^-$  and  $\text{OH}^-$  between the solution and the cement paste. Such counter diffusion can be expected in the case of NaCl additions as well. Diffusion coefficients for the cations are lower than those for the associated chloride ions since the hydrated cement behaves as an electro-positive semi-permeable membrane [26]. Hence, the alkali ion migration is much slower than that of chlorides, consequently for the period of testing (210 days), a considerable change of alkali ions concentration cannot be expected (as demonstrated in Fig. 6b–d) for sodium, potassium and magnesium).

Cations, like  $\text{Na}^+$  (along with  $\text{K}^+$ ,  $\text{Mg}^{2+}$ , etc.), will migrate towards the negative pole of the cells (the negative pole being initially with high concentration of NaCl). However, such enhanced transport is only minor for sodium in the specimens under pulse DC whereas potassium and magnesium concentrations were maintained relatively constant in all sections (Fig. 6). On one hand, this migration could be favourable if steel was embedded in the concrete, as it is supposed that alkali ions will accumulate on the steel surface. On the other hand, an increased accumulation of alkalis will cause, already mentioned in the introduction, side effects such as reduction in bond strength between the steel reinforcement and concrete. In the specimens under pulse current, the electrical pulse will enhance the electro osmotic effects and hence withdraw water

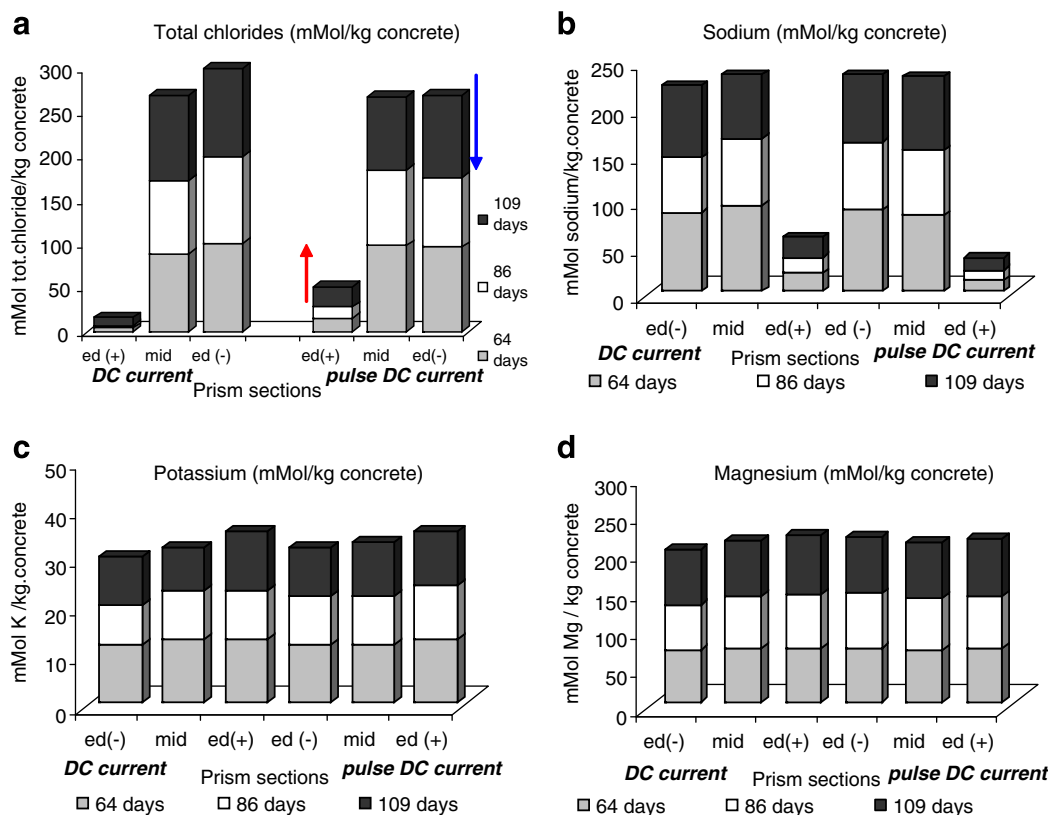


Fig. 6. Total chloride (a), sodium (b), potassium (c) and magnesium (d) concentration in mMol per dry concrete weight at the relevant sections of specimens DN under steady (left of the plots) and pulse DC current (right of the plots), derived by drilling cores in these sections.



to the negative pole in the system. A possible mechanism here is transport of  $\text{Na}^+$  ions with a water molecules hydration shell.

All aforementioned mechanisms and hypothesis aim at establishing a correlation between electrical properties of concrete with the changes in chemical composition and microstructure of the materials under various external influences, including the effect of CP current. However, a through and fundamental understanding and possible solutions for effective performance of CP technique remain to be solved. A clear statement though can be suggested for the microstructure of the concrete material and the positive or negative aspects of these factors. The presence of chloride will induce decrease in porosity and a finer pore size distribution since chloride binding leads to the formation of chloro-complexes in the capillary pores. As reported in [24], the C–S–H morphology differs in the mortars with or without chloride additions. In the chloride-free mortars, C–S–H gel is of fibrous or needle shape, accompanied by a coarse pore structure. In contrast, the chloride-contaminated mortars exhibit denser C–S–H gel and a finer pore size distribution. Similar observations are also reported by the present authors [9,27].

### 3.4. Microstructure observations

The development of the pore structure in hardening concrete is fundamental to its mechanical behaviour when exposed to aggres-

sive environments. It determines the diffusion characteristics and consequently the rate of aggressive ions penetration into the bulk material, followed by further interactions, chemical and physico-chemical alterations in the concrete matrix. Electrical current flow (as in CP applications) will additionally affect the material structure (including pore structure) and the engineering properties of concrete, which will be elaborated in what follows.

The electrolytic path in concrete systems is dependent on the kinetics of aggressive ions transport mechanisms, the latter affected by pore size distribution and pore connectivity. Figs. 7, 8 and 10 present the pore size distribution and the critical pore size of the investigated specimens. The critical pore size is a unique transport length scale of major significance for permeability properties. It is generally accepted that the smaller the critical pore size, the finer the pore structure. The critical pore size corresponds to the inflection point of the opening distribution curve (Figs. 7, 8, 10 and 12, right). The inflection point is reflected by the peak of the derivative curve of the opening distribution curve (which is the pore area fraction after opening operation vs size of structuring element; for more details on these techniques, see [29]).

Relevant to morphological aspects of the pore structure and ion transport, a characterizing parameter, the so-called pore distribution density (PDD) is implied in the microstructural investigations for all specimens in the present study. The PDD is a

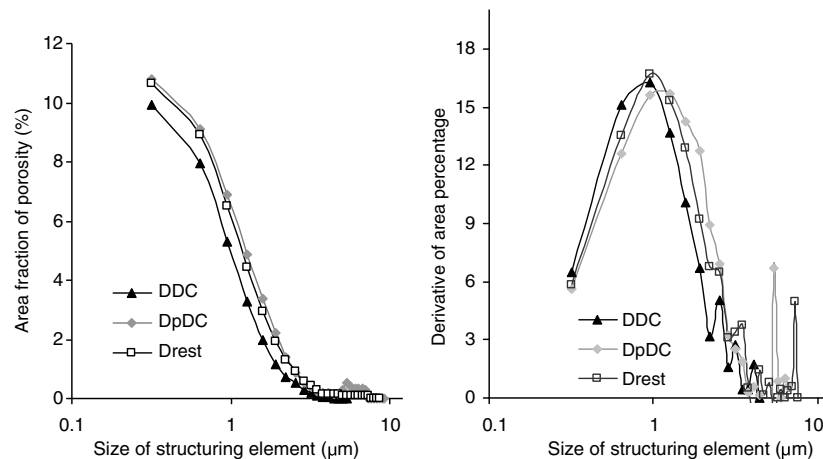


**Fig. 7.** Pore size distribution and critical pore size (peak of the curves in the right figure) for specimen D under various conditions, no-current (denoted as 'rest'), pulse (denoted as pDC), and steady (denoted as DC) current, respectively at 210 days of age.

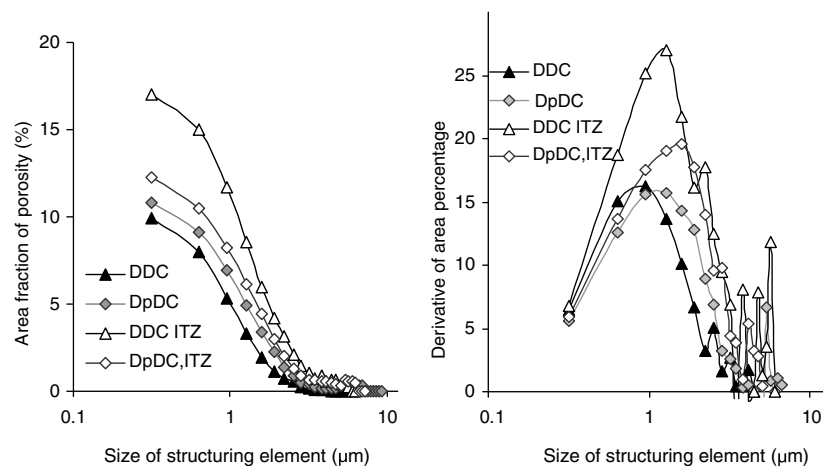


**Fig. 8.** Pore size distribution and critical pore size for the bulk matrix and ITZ regions (DDC ITZ and DpDC, ITZ) for specimen D under pulse (denoted as pDC), and steady (denoted as DC) current, respectively at 210 days of age.

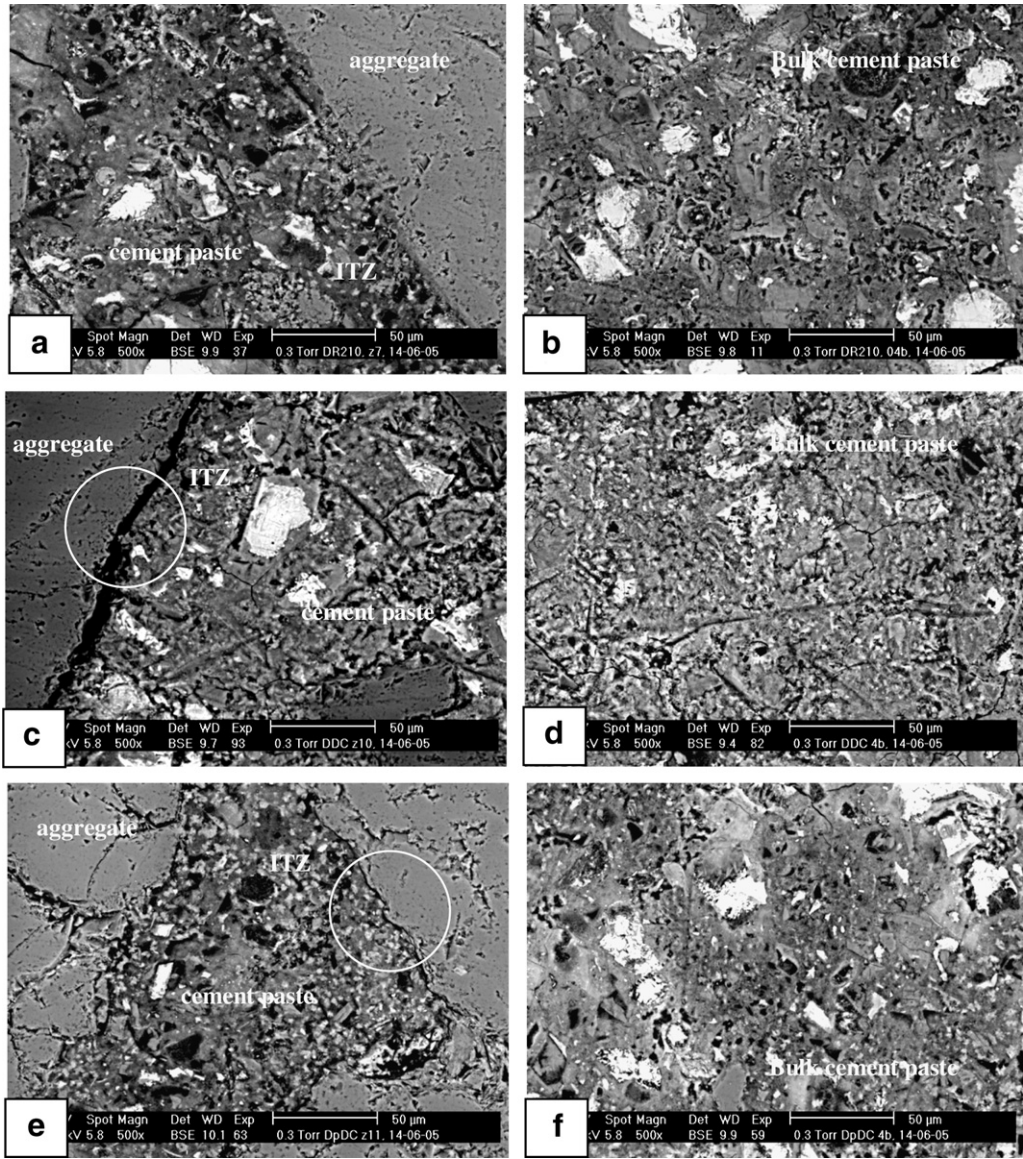


Fig. 9. The interfacial transition zone (ITZ) cement paste/aggregate and the bulk matrix in specimens Drest (a, b), DDC (c, d) and DpDC (e, f). The ESEM image magnification is 500× (210 days).

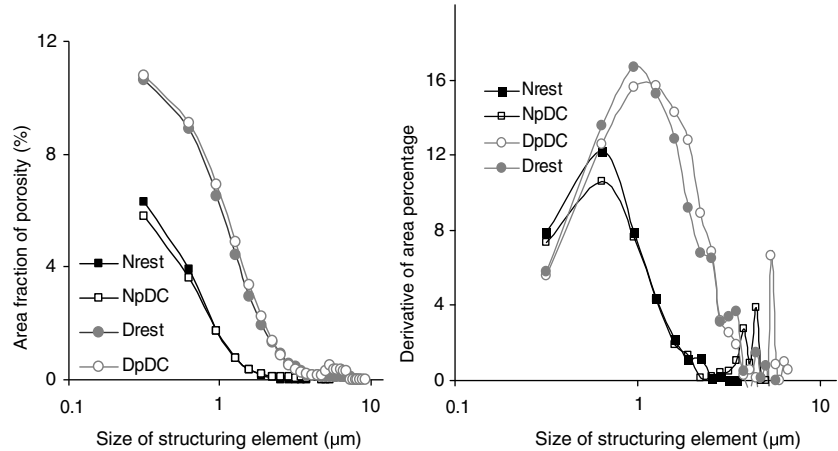
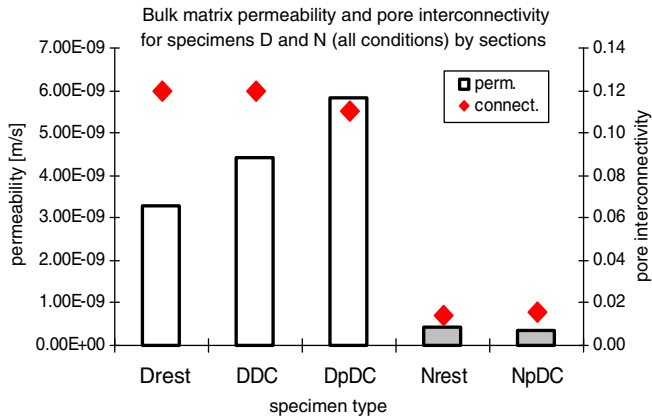


Fig. 10. Pore size distribution and critical pore size (peak of the curves in the right figure) for specimens N and D in rest conditions (denoted as Nrest, Drest) and pulse DC conditions (denoted as NpDC and DpDC), at 210 days of age.



**Fig. 11.** Bulk matrix permeability and pore interconnectivity for specimens group D in rest (Drest), steady DC (DDC) and pulse DC (DpDC) current and specimens N in rest (Nrest) and pulse DC current (NpDC) conditions.

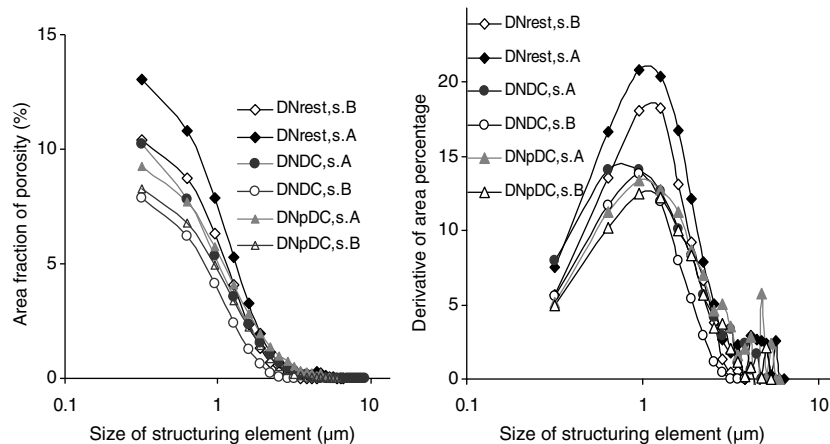
three-dimensional parameter, derived from the skeleton length of pore features, observed on two-dimensional section images. The PDD is strongly related to water permeability and is found to have higher correlation with ion transport than the conventional parameters for pore structure characterization (such as porosity, critical pore size). For more details on microstructure analysis, related definitions and measurement procedures, see [11,28–30].

Table 4 presents summarized data for porosity, critical pore size, permeability and connectivity for all investigated specimens

at 210 days of age (please see Table 1 and Section 2.1 for specimen designation and relevant abbreviations). The DC current regime causes an obvious decrease in total porosity for all conditions. Comparing specimens D and N with specimens DN allows determination of the influence of current flow on concrete microstructure separately, apart from the combined effects of concentration gradient and ion migration, (since specimens D and N have the same concrete mixture through the whole length (volume) of the specimen in contrast to specimens DN).

Fig. 7 reveals the decrease of porosity in specimen D under steady current (DDC) and almost equal porosity for specimens D in rest and pulse DC conditions (Drest and DpDC), however accompanied by a coarser pore structure in pulse DC conditions (critical pore size for DpDC is 1.268  $\mu\text{m}$ ) than no current conditions (Table 4, Fig. 7 (right)). Along with refined bulk porosity, the DC current causes increased heterogeneity in the concrete matrix, evidenced by the microstructure analysis in the bulk material and in the interfacial transition zone (ITZ) of cement paste/aggregate.

The analysis in ITZ refers to investigation of the 50–80  $\mu\text{m}$  cement paste zone, adjacent to the aggregate particle. Fig. 8 reveals the significant difference in porosity bulk ( $\sim 9\%$ ) and porosity in the ITZ region ( $\sim 17\%$ ) for specimen D under steady DC in contrast to more uniform structural performance for the specimen under pulse DC (DpDC), exhibiting bulk porosity of  $\sim 10.8\%$  and ITZ porosity of  $\sim 12.2\%$ . Critical pore size for both conditions in the ITZ region (compared to bulk matrix) is increased from 0.951 to 1.268  $\mu\text{m}$  for DC conditions and from 1.268 to 1.584  $\mu\text{m}$  for pulse DC conditions.



**Fig. 12.** Pore size distribution and critical pore size (peak of the curves in the right figure) for specimens DN by sections (s. A and s. B) for rest, steady DC and pulse DC conditions at 210 days of age.

**Table 4**

Summarized data for structural parameters for all specimens and sections

	Rest	DC	Pulse DC	Rest	DC	Pulse DC			
	Drest	DDC	DpDC	DNrest s. A	DNrest s. B	DNDC s. A	DNDC s. B	DNpDC s. A	DNpDC s. B
Porosity bulk (%)	10.64	9.92	10.8	13.07	10.42	10.20	7.88	9.27	8.25
Porosity ITZ (%)	11.20	17.03	12.2						
Critical pore size (mm)	0.95	0.95	1.27	0.95	1.27	0.95	0.95	0.95	1.27
Pore connectivity (PDD)	0.12	0.12	0.11	0.10	0.09	0.35	0.07	0.10	0.12
Permeability (m/s)	3.3e–09	4.4e–09	5.8e–09	4.6e–09	5.5e–09	1.1e–09	1.7e–09	2.4e–09	4.1e–09
	Nrest	NDC	NpDC						
Porosity bulk (%)	6.300		5.810						
Critical pore size (mm)	0.634		0.634						
Pore connectivity (PDD)	0.014		0.016						
Permeability (m/s)	4.3e–10		3.4e–10						

The most significant side effect of current flow (along with densification of the bulk porosity) is enlarging the interfacial gap between aggregate and cement paste in DC conditions – Fig. 9, while the pulse DC has minor influence on this weak zone and specimens behave similarly to rest conditions (compare Fig. 9a, c and e).

Similarly to specimens D, for the N specimens, the current flow causes decrease in the total porosity. In addition to the effects of current flow, specimens N exhibit denser pore structure as result of the influence of NaCl (as discussed in the above sections) and lower critical pore size, compared to specimens D – Table 4. Fig. 10 illustrates the previous observation, presenting a comparison of porosity and pore distribution density for specimens N and D in rest and pulse DC conditions.

Along with porosity and critical pore size, structural parameters as permeability and pore connectivity were derived for all specimens according to the above described techniques. The pore connectivity and permeability are directly related to ion transport and electrical properties, respectively. Fig. 11 presents the summarized data for these parameters for specimens D and N (no concentration gradient) and specimens under current flow (DDC, DpDC and NpDC). As seen from the plot, specimens N exhibit significantly lower values of permeability and connectivity, compared to specimens D, which correspond well to the lower electrical resistivity values for the latter (Fig. 2) and the pore structure characteristics (Table 4 and Fig. 10). The data for specimens N in Fig. 11 reflect the minor effects on the bulk matrix of the pulse current in specimens N, additionally supported by the derived conventional parameters (critical pore size for rest and pulse conditions  $0.634\ \mu\text{m}$  and similar porosity – Table 4). The specimens from group D vary in pore connectivity and permeability depending on technical conditions. Despite the almost equal porosity ( $\sim 10\%$ ) for rest (Drest) and pulse DC (DpDC) conditions, specimen DpDC has higher permeability, corresponding to the lowest electrical resistivity in the group of D specimens (Fig. 2). The higher permeability of specimen DDC (compared to Drest) and almost equal connectivity, counteract the lower porosity of specimen DDC (Fig. 7), hence the latter shows higher electrical

resistivity (Fig. 2), compared to rest and pulse DC conditions of D specimens.

The above observations generally hold for the specimens DN as well. The derived structural parameters, reflecting the properties of the bulk matrix in these specimens, are additionally influenced by the ion transport due to concentration gradient only (specimen DN in rest conditions) or due to concentration gradient and ion migration (specimens DNDC and DNpDC). Fig. 12 presents the pore size distribution and critical pore size for sections A (initially free of NaCl) and sections B (initially cast with NaCl) for specimens DN in all conditions i.e. rest, steady DC and pulse DC (as aforementioned in Section 2.1, sections A (or s. A) denote for averaged microstructural parameters for sections A3 and A(ed+), while sections B (or s. B) represent averaged values for B3 and B(ed–), Table 1). Sections A of all specimens DN exhibit higher porosity, compared to s. B in the same specimens (as consequence of induced hydration in the B sections as already discussed above). The trend of increased structural heterogeneity (as observed and discussed above for specimens D and N) is more pronounced in the specimens under steady DC: porosity of s. A  $\sim 10.2\%$ , s. B  $\sim 7.8\%$ , while specimens under pulse DC present more uniform pore structure – porosity s. A  $\sim 9.2\%$ , s. B  $\sim 8.2\%$ . The result is attributed to current-induced micro-cracking and enlarged gap between aggregate and cement paste in DC conditions (Fig. 13), compared to rest and pulse DC, similarly to those observed in specimens D and N (Fig. 9).

Despite the higher porosity in s. A of specimen DNrest ( $\sim 13\%$ , compared to  $10.4\%$  for s. B), the electrical resistivity recorded for s. B of these specimens is significantly lower (Fig. 2). The fact can be attributed to the combined influence of: structural parameters – permeability in s. A is lower (Fig. 14), ion concentrations in s. A of specimen DN rest is significantly lower as well (chloride and alkali – Fig. 5). Hence, the combination of higher permeability and higher chloride and alkali concentrations in s. B of specimen DNrest determine lower electrical resistivity of these sections, compared to s. A (Fig. 2).

In the DN specimens under current flow, the steady current yields a much higher extent of structural heterogeneity in the

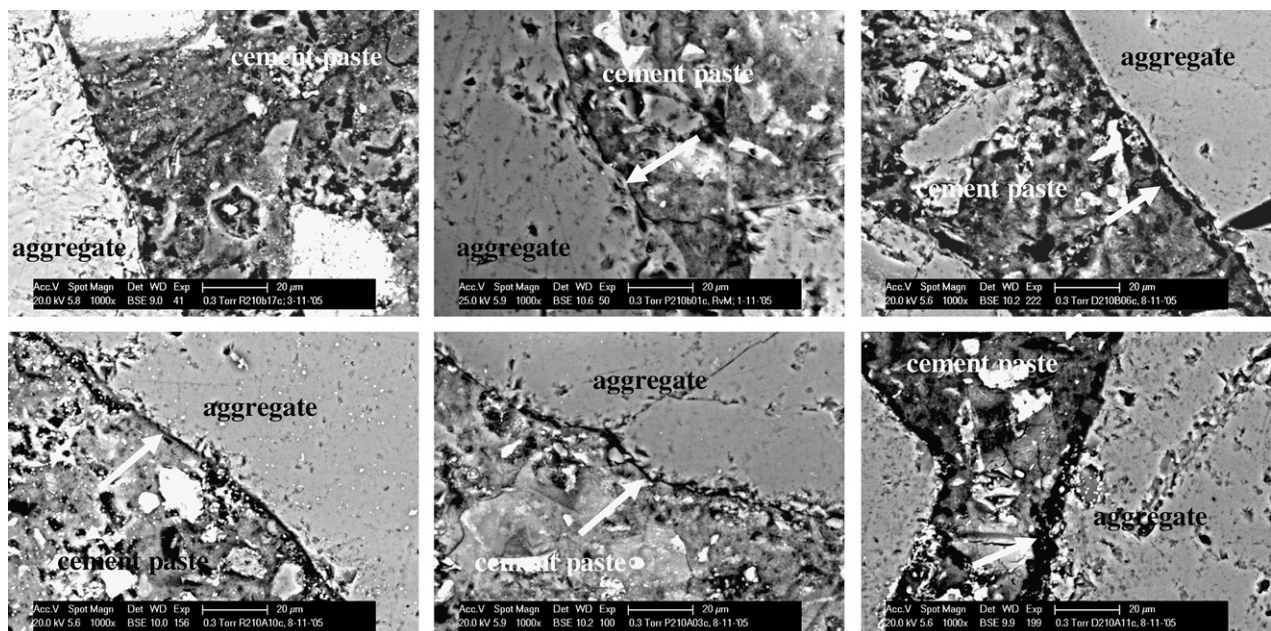
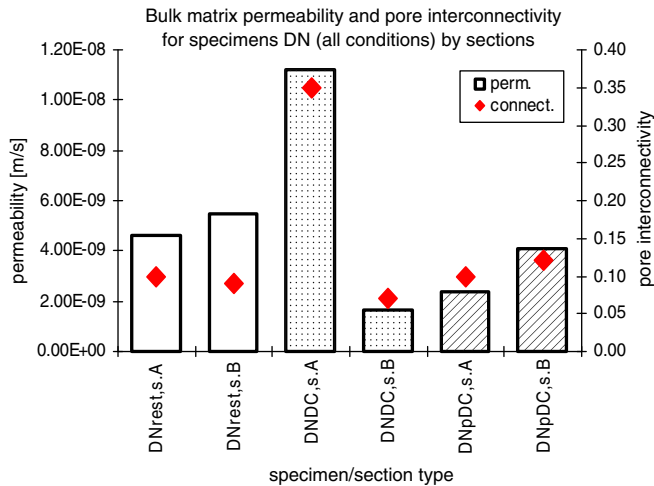


Fig. 13. The interfacial transition zone (ITZ) between cement paste and aggregate in section B (top row) and section A (bottom row) of specimen DN in rest (left), under pulse DC (middle) and under steady DC (right) conditions. The SEM image magnification is  $1000\times$ .





**Fig. 14.** Bulk matrix permeability and pore interconnectivity by sections for specimens group DN in rest (DNrest), steady DC (DNDC) and pulse DC (DNpDC) current conditions.

material, supported by the largely diverging values in electrical resistivity (Fig. 2) and corresponding well to the derived values for pore connectivity and permeability (Fig. 14). In contrast, the pulse current induces only minor changes in the pore structure (Figs. 12 and 14), and the different sections exhibit similar resistivity (Fig. 2). Therefore, pulse DC is beneficial for the bulk matrix properties, since it is promoting ion transport (Fig. 6) and current flow in the system on one hand and on the other hand it maintains structural parameters similar to that in no-current condition (Fig. 14).

The s. B in pulse condition have higher permeability than the counterpart in steady current condition and the latter is of much higher structural heterogeneity with respect to permeability properties (compare values for sections A and B in specimen DNDC, Fig. 14). Although the current flow decreases total porosity in the s. B of DNDC and DNpDC specimens (Fig. 12), the gap between cement paste and aggregate (Fig. 13) counteract the positive effects of lower porosity, resulting in a lower resistivity at section B3 for specimen DNDC (Fig. 2). The phenomena is more pronounced under steady DC conditions, attributed to comparatively larger gap in DNDC (between 2 and 6  $\mu\text{m}$  for DC and 1–3  $\mu\text{m}$  for pulse DC – Figs. 9 and 13), resulting in lower electrical resistivity in section B3 for DC, compared to section B3 for pulse DC. The section B4 in the steady current condition shows highest resistivity among all the sections of the specimens (Fig. 2), attributed to the highest amount of hydrated water (Fig. 4), lowest porosity (7.8%), connectivity (0.07) and permeability ( $1.68\text{e}^{-09}$ ) in this section (Figs. 12 and 14).

#### 4. Conclusions

In conclusion, this contribution explores the effects of pulse and steady current on material structure and electrical properties of concrete specimens. The research reveals that the pulse current is less detrimental to concrete microstructure and beneficial for electrical properties and ion transport mechanisms. A steady current (as normally used in conventional ICCP applications) tends to bring about unfavourable modifications of the material structure both in the bulk (reducing porosity) and in the interfacial transition zone (enlarging the gap at aggregate surface) to a significant extent, leading to a higher level of structural heterogeneity of the materials.

In addition steady current yields non-uniform electrical properties and thereby results in disturbance of the electrolytic path in the materials under study. Both current regimes reduce the portion of connected conductive paths in the material microstructure and thereby increase the total electrical resistivity. However, in case of pulse regime with alternating periods of 'on' and 'off' current, there is a favourable mechanism of charge–discharge cycling, and the ions are prevented from 'piling up'. Hence the pulse regime fosters ion migration mechanisms.

This comparison study demonstrates that pulse current can efficiently reduce the negative effects of steady current applications, evidenced by relatively uniform resistivity in all sections of the concrete prisms. Microstructure observations and chemical analysis reveal the underlying mechanisms to be a more homogeneous material microstructure (including slightly refined pore structure), a dense ITZ (small gap) structure, and promoted ion and water transport. This promotes favourable trends with respect to the electrolytic paths in the concrete systems. The positive effects of these chemical and microstructure changes account for achieved better global performance of the concrete materials.

#### References

- [1] Glasser FP. The alkali-silica reaction in concrete. In: Swamy RN, editor. New York: Van Nostrand Reinhold; 1992. p. 30–53.
- [2] Pedeferrri P. Cathodic protection and cathodic prevention. *Construct Build Mater* 1996;10:391–402.
- [3] Ishii K, Seki H, Fukute T, Ikawa K. Cathodic protection for prestressed concrete structures. *Construct Build Mater* 1998;12:125–32.
- [4] Chang JJ. A study of the bond degradation of rebar due to cathodic protection current. *Cem Concr Res* 2002;32:657–63.
- [5] Koleva DA, Hu J, Fraaij ALA, Stroeven P. Influences of chloride ions on plain and reinforced mortars investigated by combined microstructure and electrochemical approaches. *EUROCORR* 2005, Paper No.: 0-213-K.
- [6] Koleva DA, Hu J, Fraaij ALA, van Beek K. Concrete behaviour under pulse and conventional cathodic protection current, *Proceedings of Australian Corrosion Association. CAP05*; November 2005, Gold Coast, Australia.
- [7] Berkeley KGC, Pathmanaban S. Cathodic protection of reinforcement steel in concrete. Butterworths & Co. Ltd.; 1990.
- [8] Koleva DA. Corrosion and protection in reinforced concrete. Pulse CP: and improved, cost-effective alternative. Delft; 2007. ISBN 978-90-9021924-0; TU Delft.
- [9] Koleva DA, Hu J, Fraaij ALA, van Breugel K, de Wit JHW. Microstructural analysis of plain and reinforced mortars under chloride-induced deterioration. *Cem Concr Res* 2007;37:604–17.
- [10] Serra J. Image analysis and mathematical morphology. London: Academic Press; 1982.
- [11] Hu J, Stroeven P. Application of image analysis to assessing critical pore size for permeability prediction of cement paste. *Image Anal Stereol* 2003;22:97–103.
- [12] Whittington HW. The conduction of electricity through concrete. *Mag Concr Res* 1981;33:114.
- [13] Polder RB. Chloride diffusion and resistivity testing of five concrete mixes for marine environment. In: *Proceedings of RILEM. International workshop on chloride penetration into concrete*, St-Remy-les-Chevreuses; October 15–18, 1995.
- [14] Monfore GE. The electrical resistivity of concrete. *J PCA Res Dev Lab* 1968;10(2):35–48.
- [15] Liu X. Application of the Nernst–Einstein equation to concrete. *Cem Concr Res* 1997;27:293–302.
- [16] Andrade C, Sanjuan MA, Alonso MC. Measurement of chloride diffusion coefficient from migration tests. *CORROSION/93*, Paper No.: 319, NACE; 1993.
- [17] Gaal G. Prediction of deterioration of concrete bridges. Delft, Delft University Press; 2004.
- [18] Bungle JH. Testing of concrete in structures. 2nd ed. NYNew York: Chapman & Hall; 1989.
- [19] Broomfield JP, Rodriguez J, Ortega LM, Garcia AM. Corrosion rate and life prediction for reinforced concrete structures. In: *GEOCISA Spain, structural faults and repairs symposium*; June 1993.
- [20] Lyublinski EY. Cathodic protection of steel in reinforced concrete with electroosmotic treatment. US Patent 6,419,816; 2002.
- [21] Basheer PAM. Concrete science. Norwich: Noyes/William Andrew; 2001. [Chapter 16].
- [22] Song G. Equivalent circuit model for AC electrochemical impedance spectroscopy of concrete. *Cem Concr Res* 2000;30:1723–30.
- [23] Reddy B, Glass GK, Lim PJ, Buenfeld NR. On the corrosion risk presented by chloride bound in concrete. *Cem Concr Comp* 2002;24:1–5.
- [24] Suryavanshi AK, Scantlebury JD, Lyon SB. Pore size distribution of OPC & SRPC mortars in presence of chlorides. *Cem Concr Res* 1995;25:980–8.

- [25] Beaudoin J, Marchand J. Concrete science. Norwich: Noyes/William Andrew; 2001. [Chapter 14].
- [26] Kondo R, Satake M, Ushiyama H. The cement association of Japan, 28th General Meeting; 1974. p. 41.
- [27] Koleva DA, Hu J, Fraaij ALA. Durable building technology benefiting electrochemical methods as a preventive. In: Brebbia CA, DeGiorgi VG, Adey RA, editors. Simulation of electrochemical processes, vol. 48. (UK)UK: WIT Press; 2005. p. 87–97. May 2–4.
- [28] Katz AJ, Thompson AH. Quantitative prediction of permeability in porous rock. *Phys Rev B* 1986;34:8179–81.
- [29] Hu J. Porosity of concrete – morphological study of model concrete. Delft University of Technology. Rotterdam: OPTIMA Grafische Communicate; 2004.
- [30] Scrivener KL. Backscattered electron imaging of cementitious microstructures: understanding and quantification. *Cem Concr Comp* 2004;26:935–45.